第29卷 第10期　　焊　接　学　报　　Vol. 29　No. 10
2008年10月　　TRANSACTIONS OF THE CHINA WELDING INSTITUTION　　October　2008

TC4表面反应电火花强化层物相及磨损行为分析

马跃进[1,2]，　李午申[1]，　郝建军[2]，　白庆华[2]，　刘洪杰[2]
(1. 天津大学 材料科学与工程学院, 天津　300072;
2. 河北农业大学 机电工程学院, 河北 保定　071001)


马跃进

摘　要: 利用DZ—1400型电火花沉积/堆焊机, 以工业纯钛TA_2为电极, 以工业纯氮为保护气和反应气, 在TC4钛合金试件表面上制备了TiN/Ti复合涂层。利用X射线衍射仪分析了放电电容、输出电压、脉冲频率对涂层物相的影响, 利用MH—6型显微硬度计测定涂层断面不同区域的显微硬度, 利用KYKY2800扫描电镜观察涂层组织结构和磨损形貌, 采用MS—T3000型球—盘式摩擦磨损试验仪测试涂层的摩擦系数和磨损失重。结果表明, 涂层中物相种类随放电电容、输出电压、脉冲频率的不同而变化。涂层组织致密, 与基体之间形成冶金结合, 涂层显微硬度呈梯度变化, 涂层摩擦系数小, 耐磨性好。

关键词: 反应电火花沉积; 物相; 磨损; 复合涂层; 钛合金
中图分类号: TG174.44　　文献标识码: A　　文章编号: 0253—360X(2008)10—0021—04

0　序　　言

钛合金作为一种新型的结构材料, 因其质量轻、比强度高、耐蚀性好等优点, 在冶金、机械化工和航空航天领域都获得广泛应用[1,2]。但是钛的硬度较低, 摩擦系数大, 耐磨性很差, 易与对磨材料发生粘着磨损, 造成零件的早期失效。反应电火花沉积是一种无应力、无变形的表面强化工艺, 它把电火花沉积技术和反应合成技术有机地结合起来, 通过电火花沉积的火花放电使作为反应组元的保护气体被击穿电离, 并在 10^{-5} ~ 10^{-6} s内使电极与工件接触处达到8 000 ~ 25 000 ℃的高温, 促使熔融的电极材料、基体材料与电离的反应组元保护气体发生反应生成金属基陶瓷涂层, 从而使工件的物理、化学和力学性能得到改善[3]。实践表明, 利用反应电火花沉积技术在钛合金表面制备TiN/Ti复合涂层, 可极大地改善钛合金的表面性能[3,4]。研究反应电火花沉积工艺参数对涂层性能影响规律, 是获得优质涂层的依据。为此, 针对常规TiN制备中存在工艺复杂、成本高、厚度小等问题, 利用反应电火花沉积技术[5], 采用DZ—1400型电火花沉积/堆焊机, 以工业纯钛TA_2为电极材料, 以工业氮气为保护气体和反应气体, 在TC4钛合金基体上制备了TiN/Ti复合涂层, 并对涂层物相及其磨损行为进行了初步研究。

1　试验方法

试验所用基材为TC4钛合金, 其化学成分(质量分数, %)为Al 6.1, V 3.8, Fe 0.3, Si 0.1, C 0.1, O 0.15, N 0.05, H 0.015, 其余为Ti, 热处理状态为退火态。电极材料为ϕ3 mm的工业纯钛TA_2, 其化学成分(质量分数, %)为C 0.1, O 0.25, Fe 0.3, 其余为Ti。作为反应组元的保护气体采用纯度不低于99.5%的工业氮气。

试样尺寸为ϕ30 mm×4 mm的TC4钛合金圆片, 依次经过200, 400, 800和1 200号砂纸打磨处理, 在丙酮溶液中超声清洗20 min后吹干, 然后用DZ—1400型电火花沉积/堆焊机进行强化处理。根据经验, 选择氮气流量10 L/min, 比沉积时间3 min/cm^2, 电极转速2 400 r/min。根据设备可调范围, 放电电容、输出电压、脉冲频率的选择如表1所示。

采用D/max—RA型X射线衍射仪分析涂层物相组成, 采用MH—6型显微硬度计测定涂层断面显微硬度, 利用KYKY2800扫描电镜观察涂层组织结构和磨损形貌。采用MS—T3000型球—盘式摩擦磨损试验仪测试涂层的摩擦系数和磨损失重。摩擦副为ϕ3 mm的65Mn圆柱(850 ℃加热, 分级淬火和180 ℃回火), 载荷50 N, 转速1 000 r/min。试验温度为25 ℃, 摩擦为干摩擦。用电子分析天平(测

收稿日期: 2008—01—24
基金项目: 河北省自然科学基金资助项目(E2007000566)

表 1 沉积工艺参数

Table 1 Processing parameters for deposition

编号	放电电容 C/μF	输出电压 U/V	脉冲频率 f/Hz
1	50	90	1 000
2	100	90	1 000
3	100	90	1 000
4	100	160	1 000
5	100	90	500
6	100	90	1 000

量精确度为0.1 mg) 称量样品和圆柱磨损先后的重量来计算磨损失重,每次称重前都将样品和圆柱用丙酮超声波清洗并烘干。

2 结果与分析

2.1 涂层物相

图1~图3 分别为 2 种放电电容(表 1 中的试验编号 1 和 2)、2 种输出电压(表 1 中的试验编号 3 和 4)、2 种脉冲频率(表 1 中的试验编号 5 和 6)条件下反应电火花沉积强化涂层的 XRD 谱。

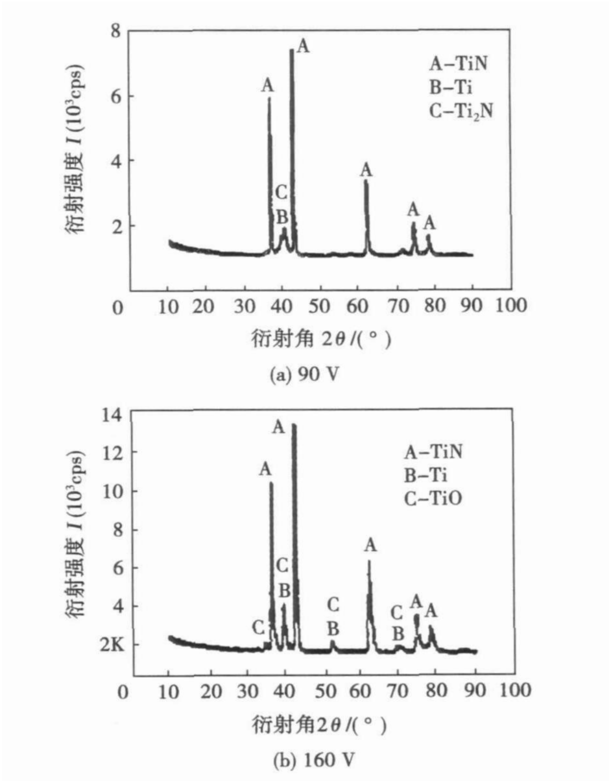

图 2 电压对涂层物相的影响

Fig. 2 Effect of operating voltage on XRD patterns

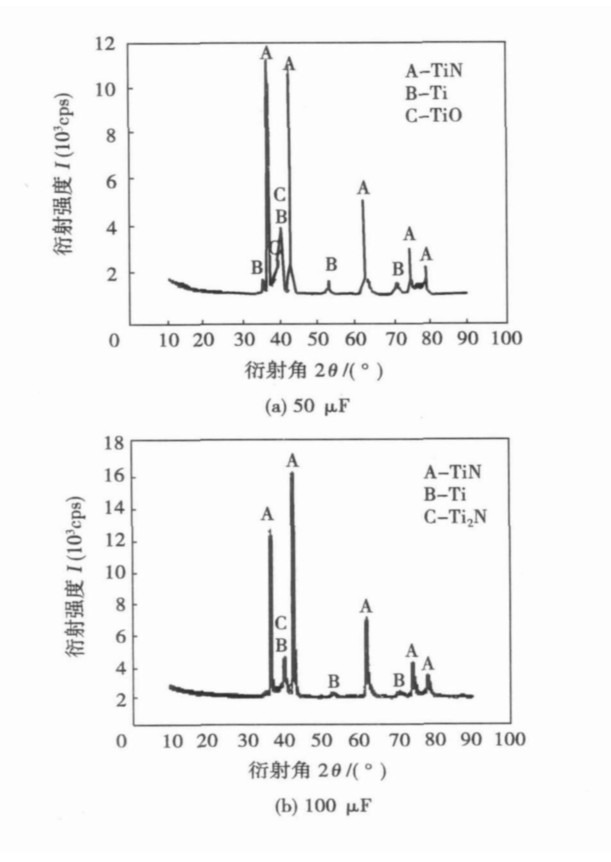

图 1 电容对涂层物相的影响

Fig. 1 Effect of discharge capacitance on XRD patterns

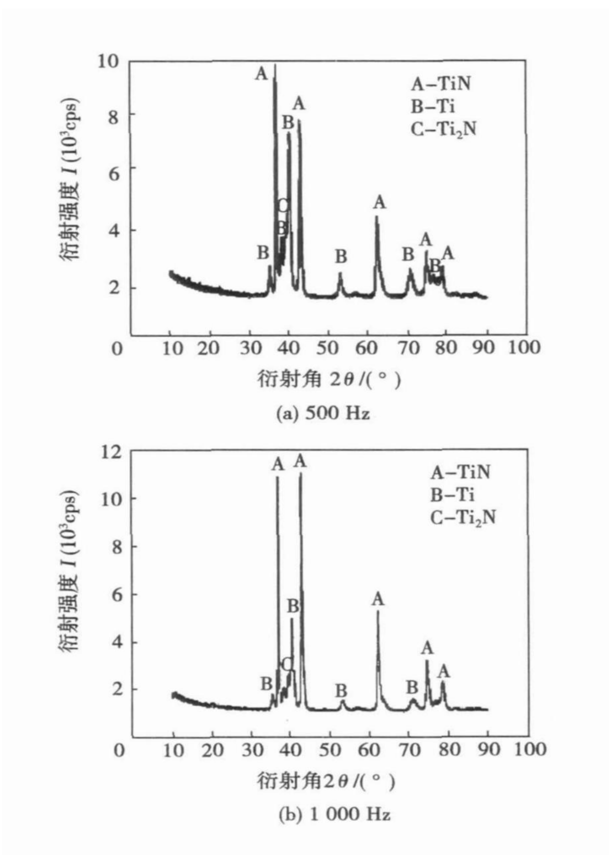

图 3 频率对涂层物相的影响

Fig. 3 Effect of frequency on XRD patterns

由图 1～图 3 可见, 不同工艺参数下, 涂层 XRD 谱中均出现钛衍射峰和较强的 TiN 衍射峰, 因此可认为, TiN 是涂层主要成分; 放电电容、输出电压、脉冲频率越大, TiN 衍射峰强度越强。但输出电压为 160 V时涂层中出现了 TiO 衍射峰; 放电电容为 50 μF时涂层中出现了TiO 衍射峰。

在反应电火花强化过程中, 旋转电极和基体之间产生火花放电, 火花放电释放的高能量($P = W \cdot f$, $W = C \cdot U^2$, P 为火花放电功率, W 为单次放电能量, C 为放电电容, U 为工作电压, f 为输出频率) 将基体熔化形成熔池, 使电极端部发生局部熔化形成熔滴。同时, 从沉积枪口喷出的氮气被电离为高活性的氮离子(N^+ 及 N^-) 和氮原子(N) , 氮离子、氮原子及未被电离的氮分子吸附在熔池液态金属表面。伴随着基体的熔化(融) , 电极熔滴的溅射和保护气体的电离, 高活性的氮等离子流通过扩散作用克服固液界面表面能进入熔池, 与熔融状态的钛在高温下化合形成 TiN ($Ti + [N] \rightarrow TiN$, $Ti + N \rightarrow TiN$, $2Ti + N_2 \rightarrow 2TiN$) , TiN 晶粒不断形核长大形成 TiN 强化层[3]。熔滴大小、熔滴温度和溅射距离是影响 TiN 反应和 TiN 晶粒生长的主要因素, W 越大, 熔滴越大, 熔滴温度越高, 溅射距离越远。P 越大, 熔池温度越高、熔融物流动性越好、熔滴溅射力越大。

温度的提高使合成 TiN 的反应速度加快, 反应时间加长, 有利于 TiN 的生成, 但温度过高将导致熔滴增大, 减小了熔滴与 N 原子的接触面积, 不利于 TiN 生成。同时, W 增大, 熔滴溅射加剧, 溅射距离增加, 从而可能导致熔滴脱离 N_2 的保护, 与空气接触发生氧化反应生成钛的氧化物, 氧化物不仅减缓了 TiN 的反应合成, 而且还抑制TiN 晶粒的生长。

在相同的充电时间内, 小电容(50 μF) 时电容两端获得的放电电压比大电容(100 μF) 高, W 大, 因此当电容为50 μF时, 涂层中出现了 TiO; 随着工作电压的增大, P 增大, 因此当输出电压为高压(160 V) 时, 涂层中出现了 TiO; 脉冲频率直接影响火花放电功率 P, P 随脉冲频率的增大而增加, 频率增大, 电极熔融速度变快, 有利于TiN 的生成和生长, 因此当放电频率为1 000 Hz时, 涂层中未出现钛的氧化物。

综上所述, 获得优良涂层的最佳工艺参数为放电电容100 μF, 输出电压90 V, 脉冲频率1 000 Hz。

2.2　涂层组织

图4 为反应电火花沉积强化涂层试样截面微观组织形貌(反应电火花沉积工艺参数为放电电容 100 μF, 输出电压90 V, 脉冲频率1 000 Hz, 氮气流量 10 L/min, 比沉积时间 3 min/cm², 电极转速 2 400 r/min) 。

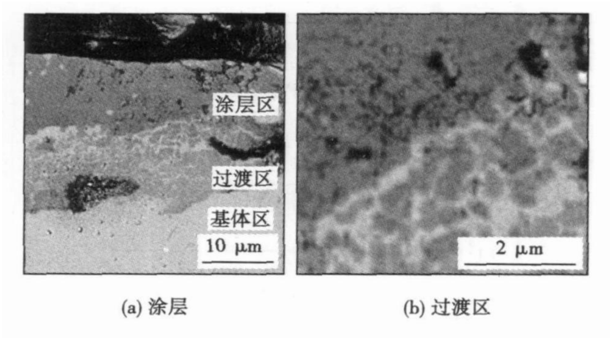

图 4　试样截面微观组织
Fig. 4　Cross section microstructure of specimen

由图4 可以看出, 涂层厚度为 20～30 μm, 试样截面可明显分成涂层区、过渡区和基体区 3 个区域, 3 个区之间没有明显界限, 结合致密, 说明涂层与基体之间形成了良好的冶金结合。

2.3　涂层硬度

图 5 为涂层截面显微硬度分布图, 由图 5 可知, 涂层表层的显微硬度最高达 1 388 HV0. 1, 约是基体硬度(220 HV0. 1) 的 6 倍以上, 这主要是由于涂层表层中有较多的 TiN 硬质相; 而过渡区硬度已下降至 500 HV 以下, 这主要是由于重复涂敷的回火作用等原因所致。

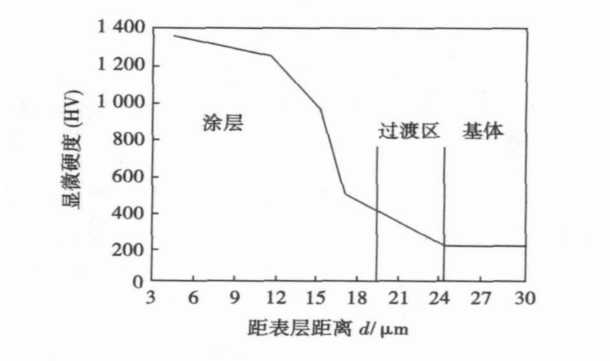

图 5　涂层显微硬度分布
Fig. 5　Microhardness curve of coatings

2.4　涂层磨损行为

图 6 为涂层摩擦系数随试验时间的变化曲线。由图6 可见, 摩擦初期, 涂层的摩擦系数相对较高, 稳定磨损期摩擦系数波动于 0. 6～0. 75 之间, 摩擦后期, 摩擦系数稍有降低。分析认为, 稳定磨损阶段, 摩擦系数波动, 可能是由于涂层中钛和 TiN 的不均匀分布造成的; 摩擦后期, 摩擦系数降低可能是由于摩擦后期磨痕加宽, 导致接触处平均应力减小所致。

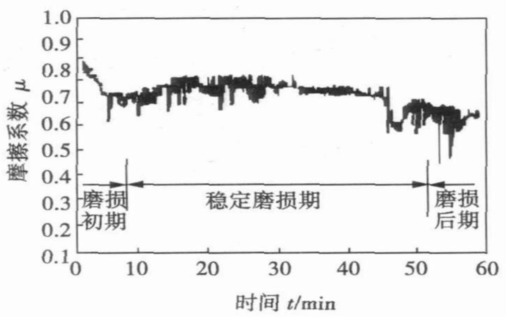

图 6 涂层摩擦系数曲线

Fig. 6 Friction coefficient curve of coatings

图7 为涂层与圆柱在相同条件下磨损失重随时间变化的关系曲线。

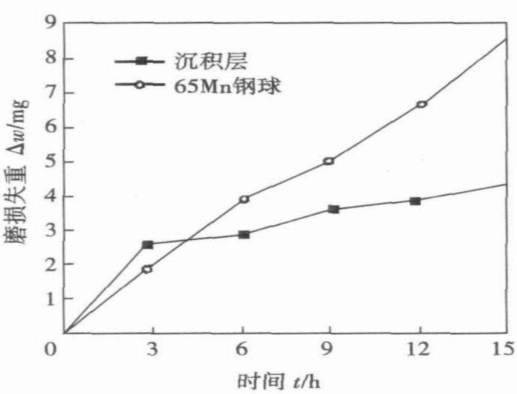

图 7 涂层与 65Mn 磨损失重对比

Fig. 7 Comparison of wearing capacity lost for coatings and 65Mn

由图 7 可以看出, 在磨损初期, 涂层的磨损失重比圆柱大; 随着时间的延长, 圆柱的磨损失重几乎呈线性增加, 而涂层的的磨损失重变化甚微。涂层表层中由于电极粘连作用含有比涂层内部较多的钛和较少的 TiN 硬质相, 因此在磨损初期, 涂层的磨损失重较大。涂层内部含有一定量的钛及部分 N 元素的缺位的 TiN 相, 使涂层的金属性增强, 韧性增强, 抗疲劳性好, 致使裂纹不易扩展, 从而有效地阻止了涂层脆裂的发生; 涂层内弥散分布的大量 TiN 硬质相起到耐磨骨架的作用以抵抗磨粒的切削、凿削、推挤和擦划; 二者的共同作用使得涂层具有较高的耐磨性能。

图8 为涂层与对比圆柱对磨后的表面磨损形貌。

由图 8 可见, 涂层结合良好, 无剥落和脱皮现象, 磨痕断断续续, 磨痕稀疏并且浅而窄, 甚至几乎看不到磨痕。而圆柱上则发现深而宽、连续、密集、方向性强的明显划痕。这充分说明反应电火花沉积层的耐磨性优于淬火回火的 65Mn 钢圆柱。

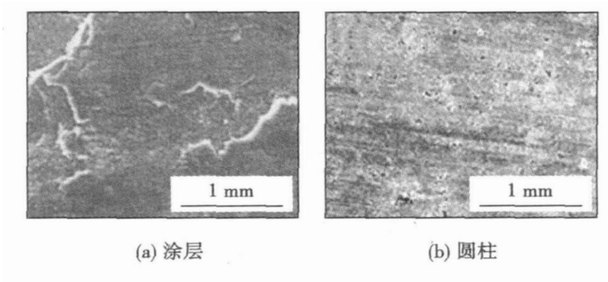

图 8 磨损形貌

Fig. 8 Wear morphology

3 结 论

(1) 利用反应电火花沉积技术, 以工业纯钛 TA_2 为电极, 氮气为反应气体和保护气体, 在 TC4 钛合金表面制备出了含 TiN 硬质相的致密、均匀、连续、与基体呈冶金结合的反应涂层。

(2) 涂层中 TiN 相是沉积过程中电极材料和基体材料 Ti 元素和保护气体 N 元素经冶金反应后生成的一种新的化合相。涂层物相受放电电容、输出电压、脉冲频率的影响。

(3) 涂层硬度随着距表面距离的增大而减小, 显微硬度最高达1 388 HV0.1, 是基体硬度的6 倍多。

(4) 涂层与基体形成冶金结合, 涂层韧性强, 摩擦系数小, 耐磨性好。

(5) TC4 表面反应电火花沉积金属基陶瓷涂层操作简单、沉积效率高、涂层性能优良, 可用于零件表面划伤、沟槽等缺陷的修复与强化。

参考文献:

[1] 何 鹏, 吴承东, 钱乙余, 等. 钛合金表面电火花沉积 WC 电极的粘连行为分析[J]. 焊接学报, 2006, 27(4): 25—28.

[2] 张春辉, 游 涛, 闫 平, 等. 钛合金表面电火花沉积强化研究现状[J]. 稀有金属快报, 2007, 36(2): 1—6.

[3] 郝建军, 黄继华, 赵建国, 等. 电火花沉积反应合成 TiN 增强金属基复合涂层[J]. 焊接学报, 2007, 28(10): 33—36.

[4] 牛金辉, 任振安, 李 欣. 氮气氛下电火花沉积 TiN 层的形成机理及微观特征[J]. 焊接学报, 2007, 28(6): 101—104.

[5] 郝建军, 马跃进, 陈志强, 等. 一种氮化钛金属基陶瓷涂层的反应电火花沉积制备方法: 中国, 200610012842.4[P]. 2006—11.

作者简介: 马跃进, 男, 1958 年出生, 硕士, 教授, 博士生导师。主要从事表面涂层制备方面的研究工作。发表论文 40 余篇。

Email: myj@hebau.edu.cn

phase with eutectoid treatment. After annealing in vacuum, the effect of big grains refinement in the fusion area was very obvious. After annealing in vacuum, the tensile strength decreased and plasticity increased a little.

Key words: TA15 alloy; hydrogen treatment; microstructure; mechanical property

Study on XRD patterns and wear behavior of TC4 coated by reactive electric-spark deposition Ma Yuejin[1,2], Li Wushen[1], Hao Jianjun[2], Bai Qinghua[2], Liu Hongjie[2] (1. School of Materials Science and Engineering, Tianjin University, Tianjin 300072, China; 2. College of Mechanical & Electronic Engineering, Agricultural University of Hebei, Baoding 071001, Hebei, China). p21—24

Abstract: TiN/Ti composite coating was deposited on TC4 titanium alloy substrate with electric-spark deposition machine modeled DZ-1400, which the commercial pure titanium (TA_2) was used for electrode and the commercial pure nitrogen gas was employed as shielding and reacting atmosphere. Effects of the parameters as discharge capacitance, output voltage and impulse frequency on X-ray diffraction (XRD) patterns of TiN /Ti composite coatings were analyzed X-ray diffractometer. The microhardness of coatings was tested with microhardness instrument modeled MH-6. The microstructures and wear morphology were investigated by scanning electronic microscope (SEM). The friction coefficient and wearing capacity lost were tested by ball-pan wear and tear gauge modeled MS-T3000. The results indicated that TiN, a new phase, was synthesized by the element of Ti and N, which come from electrode, substrate and shielding gas respectively and the coatings are mainly composed of Ti and TiN. The XRD patterns were changed with the change of discharge capacitance, output voltage and impulse frequency. An excellent bonding between the coatings and substrates is ensured by the strong metallurgical interface. The highest microhardness of coating reaches to 1 388 HV0.1, which is about six times more than that of the substrates. The friction coefficient of the coatings is small and the wear resistance is excellent.

Key words: reactive electric-spark deposition; XRD patterns; wear; composite coating; titanium alloy

Numerical simulation on stress-strain field of laser welding aluminum alloy joints with different thickness YU Shurong[1], FAN Ding[2], XIONG Jinhui[2] (1. College of Mechanical and Electrical Engineering, Lanzhou University of Technology, Lanzhou 730050, China; 2. Key Laboratory of Non-ferrous Metal Alloys, The Ministry of Education, Lanzhou University of Technology, Lanzhou 730050, China). p25—28

Abstract: By finite element code ANSYS, the 3D stress-strain fields of aluminum alloy joints in different thickness made by laser welding were simulated. In order to improve the accuracy and efficiency, transition mesh was used. The effects of temperature-dependent material parameters were considered in the model. The bilinear kinematical hardening (BKIN) was established. Proper restrictions of displacement were applied for simulating effect of clamps. The result of simulation indicates that, the stress-strain field in the thin plate is larger than the thick one. Using hole-drilling technique, the residual stress was measured. It is shown that the simulation results are in accordance with the experimental results.

Key words: aluminum alloy; laser welding; different thickness; stress-strain field; numerical simulation

Study on microstructure and properties of IRCGHAZ in WB36 steel WANG Xue[1], CHANG Jianwei[2], HUANG Guanzheng[2], ZHANG Yinglin[1] (1. School of Power and Mechanics, Wuhan University, Wuhan 430072, China; 2. Henan No. 1 Power Construction Company, Pingdingshan 467031, Henan, China). p29—32

Abstract: Microstructures and properties in the intercritical reheated coarse-grained heat-affected zone (IRCGHAZ) of WB36 (15NiCuMoNb5) steel were studied by means of thermal simulation. In particular, the forming of M-A constituent in the IRCGHAZ and its influence on the toughness were investigated. Experimental results show that the coarsing lath martensite (ML) is retained in the IRCGHAZ, however, a great deal of M-A constituents are formed in IRCGHAZ compared with the coarse grain heat-ffected zone (CGHAZ), with elongated M-A constituents distributed at ML boundaries within the prior austenite grain and necklace-like blocky M-A constituents along the prior austenite grain boundaries. The toughness of IRCGHAZ is the lowest compared with that of the CGHAZ, the second CGHAZ and SCCGHAZ, which led to the local brittleness zone in HAZ. The loss in impact value of the IRCGHAZ was due to the formation of elongated M-A constituents in the interior of the grains, but not related to the formation of necklace-like M-A constituent along the prior austenite grain boundary region.

Key words: low alloy high strength steel; inter-critically reheated coarse-grained HAZ; microstructure; brittleness; M-A constituent

Residual stress field in hole-drilling method— part II: application LI Hao, LIU Yihua (School of Civil and Hydraulic Engineering, Hefei University of Technology, Hefei 230009, China). p33—36

Abstract: Based on the modified computational model for the hole-drilling method to measure residual stresses, a new formula, considering the work-hardening layer, was developed to estimate the residual stress distribution by the relaxed strain. As an example, a 304 stainless steel specimen was submitted to a single uniform tension force, and the initial stress in the specimen was regarded as the residual stress. The relaxed strains were determined during hole drilling, and the residual stresses were introduced by two ways, in which the work-hardening layer was ignored and considered respectively. Using the relaxed strains published previously, the residual stresses in a bent 16MnR steel specimen were adopted by the same two ways as well. The accuracy of the two ways was presented by comparing the calculated residual stresses with the actual residual stresses, i. e., the given initial stresses. Furthermore, the welding residual stresses were measured in a rear axle of the vehicle. The results indicate that the work-hardening layer has an obvious influence on distribution of the residual stress, and the modified computational model is logical and feasible.

Key words: residual stress; hole-drilling method; work-hardening; relaxed strain

Impact pressure diffusion bonding on surface nanocrystallization titanium alloy/stainless steel HAN Jing, SHENG Guangmin,